◆ Research paper

DOI: 10.5281/zenodo.14025334

Monitoring Ground Deformation in Beijing and Analysis of Influencing Factors

Zheng Yunxi[1,2], Sun Jichao[1,2*]

[1]Key Laboratory of Groundwater Conservation of MWR, China University of Geosciences, Beijing, China

[2]Department of Water Resources and Environment, China University of Geosciences, Beijing, China

* Corresponding author Email: sunjc@cugb.edu.cn

Abstract: Currently, the land subsidence development in Beijing is still at a relatively high rate. It is widely believed to be caused by extensive groundwater extraction, leading to a lowering of the groundwater table and consequent land subsidence. However, precipitation and surface soil moisture are crucial components of the hydrological cycle, replenishing groundwater. Previous research has paid limited attention to the analysis of the impact of precipitation and surface soil moisture on land subsidence. Therefore, this study uses 17 scenes of Sentinel-1A data to obtain surface deformation information in the research area based on SBAS-InSAR technology. It combines surface soil moisture and precipitation data to explore their influence on land subsidence. The results indicate that the Chaoyang-Tongzhou belt experiences the most serious subsidence, with a subsidence rate reaching -144.3mm/a and a maximum cumulative subsidence of -169mm; The surface soil moisture and precipitation data show a positive correlation with land subsidence, indicating that increase in precipitation and surface soil moisture partially alleviates land subsidence; In most regions, surface soil moisture in summer and winter is negatively correlated with land subsidence, while in autumn and spring, it is positively correlated with land subsidence in most areas.

Keywords: precipitation, surface soil moisture, land subsidence, SBAS-InSAR

Introduction

Land subsidence phenomena occur widely in every region of the world, manifesting as a gradual decrease in the elevation of the Earth's surface over a certain period (Lei et al., 2016). Land subsidence affects people's production and life to varying degrees, posing threats to their lives and property. Especially in the Beijing area, land subsidence has been developing rapidly. With the introduction of the South-to-North Water Diversion Project in 2014, which alleviated the water supply shortage in Beijing, the rate of land subsidence has started to show a slowing trend (Luo, 2017). By the end of 2016, the maximum cumulative subsidence in the Beijing plain area reached 1864mm, with a maximum subsidence rate of 150mm/a, still at a relatively high subsidence rate (Cheng et al., 2016) The uneven land subsidence in the region has already had a certain impact on the construction of transportation hubs and surrounding urban areas. Phenomena such as partial building collapses, wall cracks, and damage to underground pipelines have occurred within subsidence areas (Tian et al., 2016), affecting urban construction and reducing the lifespan of urban buildings. Therefore, monitoring land subsidence in Beijing and exploring its causes are of great significance for disaster prevention and mitigation. Figure 1 shows the cracking of houses caused by land subsidence in Beijing, along with the soil layer structure of Beijing.

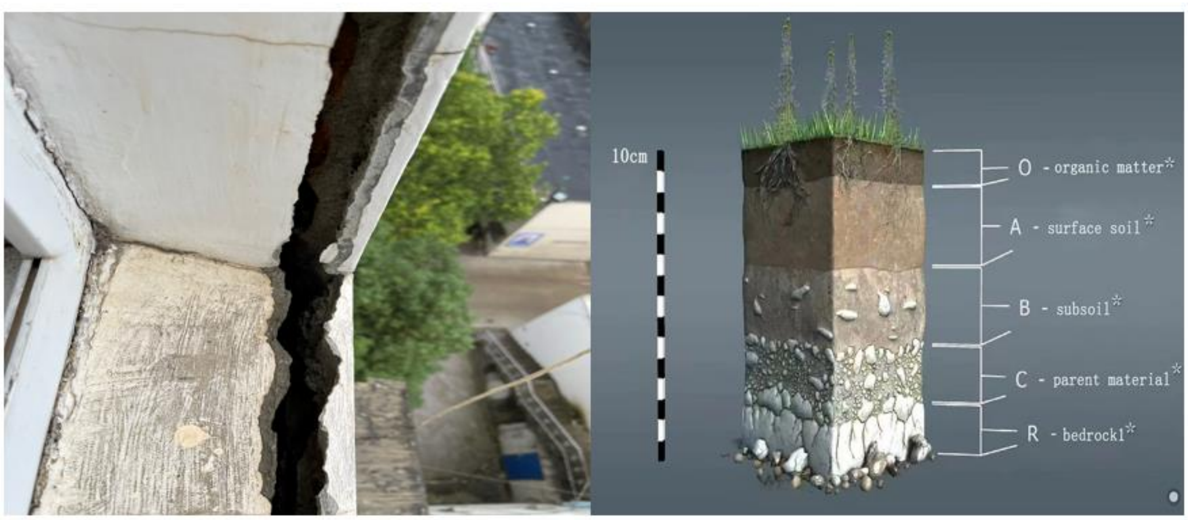

Fig. 1 The cracking of houses and soil layer structure

Currently, commonly used techniques for detecting ground deformation include leveling measurements (Chang et al., 2016; Lv et al.,2021), Global Positioning System (GNSS) monitoring (Liu et al., 2020; Sun et al.,2018), and Interferometric Synthetic Aperture Radar (InSAR) (Bayik et al., 2021),. Compared to traditional monitoring techniques, InSAR technology utilizes the phase signal of synthetic aperture radar (SAR) to obtain ground deformation information in millimeter units by subtracting the influence of other signals such as atmospheric phase, topographic phase, and orbit errors. InSAR technology has the advantages of all-weather, all-round-the-clock, wide coverage, and high precision. It has been successfully applied in various areas such as subway systems, highways, and riverbanks for subsidence analysis and identification of subsidence anomaly areas. From the perspective of overall risk management, it provides objective data analysis and technical support for scientific decision-making, rational planning, and risk control in construction projects (Kim et al.,2021),. The SBAS-InSAR technology was proposed by Bernardino and Lanari in 2002 (Berardino et al.,2002). AliMehrabi (AliMehrabi et al.,2020) utilized thresholding and SBAS-InSAR technology to analyze time-series Sentinel-1 images, elucidating the reasons for ground displacement caused by extreme floods, identifying several active motion areas, and thus determining the spatial extent of flood impact. Wang Song et al (Wang et al.,2020) conducted research on land subsidence in mining areas using SBAS-InSAR technology. The results show that rapid subsidence areas were concentrated on the surface of the goaf at the Honghui Coal Mine, coinciding with the spatial distribution of ground fissures, with a maximum cumulative subsidence of 170mm. Although the environmental restoration and management area has repaired many subsidence pits and ground fissures, it continues to subside at an annual rate of 40-50 mm. Song Yuqiao et al (Song et al.,2024) used SBAS-InSAR technology to monitor deformation around Dianchi Lake. The results indicate that the ground deformation rate in the study area was relatively high, and the degree of subsidence in industrial park construction and surface runoff areas was much greater than in other areas. Therefore, SBAS-InSAR technology has matured in monitoring land subsidence, earthquakes, landslides, and other deformation aspects and can be applied to ground deformation monitoring in the study area. Figure 1 shows the cracking of houses caused by land subsidence in Beijing, along with the soil layer structure of Beijing.

From a mechanistic perspective, land subsidence refers to the loss of surface elevation caused by the compression of the surface soil, influenced by a combination of natural and anthropogenic factors Natural influences include compaction of overlying sediments or dissolution of carbonate rocks, as well as intense movements such as tectonic activity or earthquakes (Wu et al., 2006; Yang et al.,2013). Anthropogenic influences encompass the extraction of underground fluids resources such as groundwater, natural gas, and petroleum, as well as coal mining operations. Subsidence can also occur during urban engineering construction processes, particularly in areas with soft soil where consolidation settlement may occur (Zhou et al., 2002). There are many causes of land subsidence, with previous studies indicating that excessive extraction of groundwater is a primary mechanism. Additionally, factors such as geological characteristics and engineering construction can also affect land subsidence. Dogan (Dogan et al., 2005) suggested that the extensive development of underground karst and the significant dissolution of gypsum are contributing factors to widespread land subsidence in the upper basin of the Tigris River in Turkey. Sun Jichao's (Sun,2016) research on ground sedimentation suggests that the transfer and loss of sediment are key reasons for land subsidence. E. Jian et al (E et al., 2007) believe that excessive extraction of deep groundwater is the primary cause of land subsidence. Few scholars focus on the relationship between precipitation, surface soil moisture, and changes in land subsidence.

Therefore, this study selects certain areas of Beijing as the research area, using 17 scenes of Sentinel-1A images from May 2017 to May 2018, the SBAS-InSAR monitoring technique is employed for time-series monitoring of surface deformation. The annual average deformation rate of the study area is obtained, and combined with precipitation data and surface soil moisture data within the study area, the potential impacts on land subsidence are analyzed. This provides a basis for the management of land subsidence in Beijing.

Study area.

The study area is located at the northwest edge of the North China Plain, centered at approximately 39°56'N latitude and 116°20'E longitude. It mainly includes areas such as Changping, Shun Yi, Tong Zhou, Da Xing, Fang Shan, Men Tou Gou, Hai Dian, Chao Yang, Shi Jing Shan, Feng Tai, Xi Cheng, and Dong Cheng. The terrain is higher in the northwest and lower in the southeast. Figure 2 shows the elevation map of the study area. The study area features a typical temperate monsoon climate with distinct four seasons. There are noticeable seasonal variations in wind direction, temperature, and precipitation. Summers are hot and rainy, winters are cold and dry, while spring and autumn are relatively short. Precipitation distribution throughout the seasons is uneven. Figure 3 illustrates the basic precipitation patterns in the study area from 2008 to 2022, indicating that approximately 75% of the precipitation occurs during the summer season.

The study area has been shaped by crustal movements, resulting in numerous folds and faults, as well as a significant amount of magma. Additionally, there are various landform types such as hills, intermontane basins, and low mountains. The lithology is also diverse, with various types of rocks exposed, although some strata are missing. These geological features are mainly concentrated in the northern and western mountainous regions, predominantly consisting of igneous rocks, followed by metamorphic and sedimentary rocks.

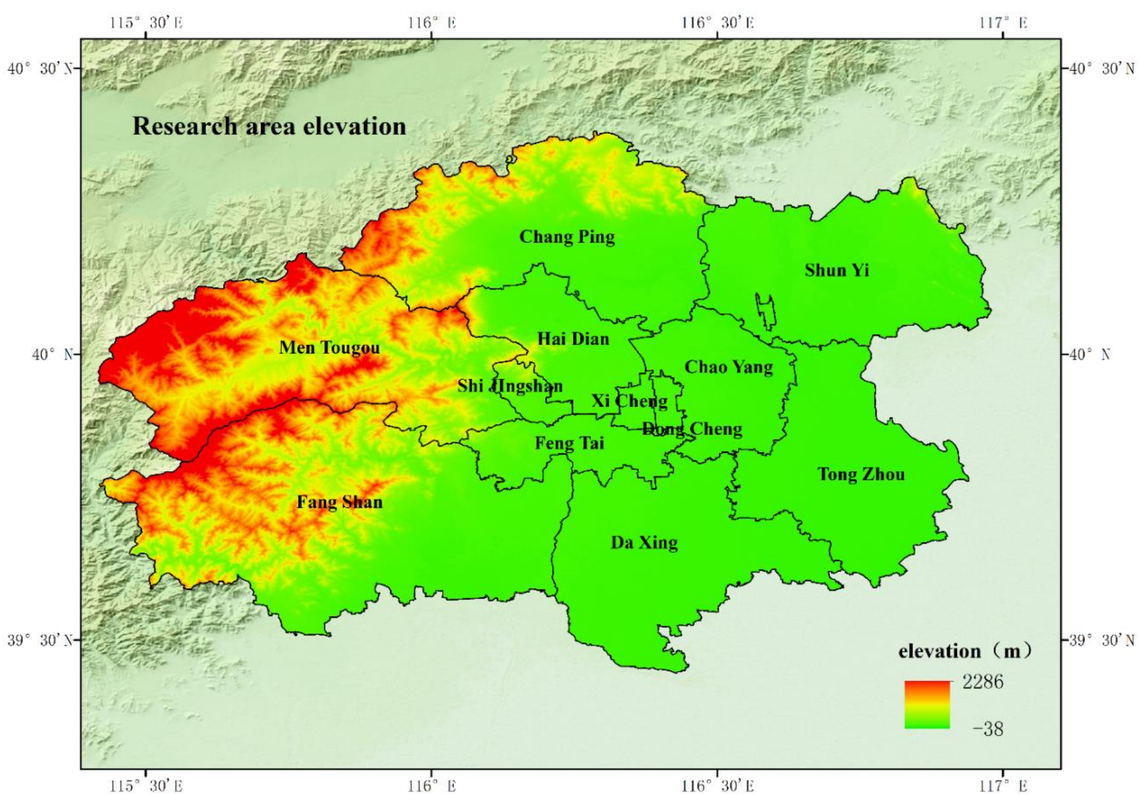

Fig. 2 Research Area Elevation Chart

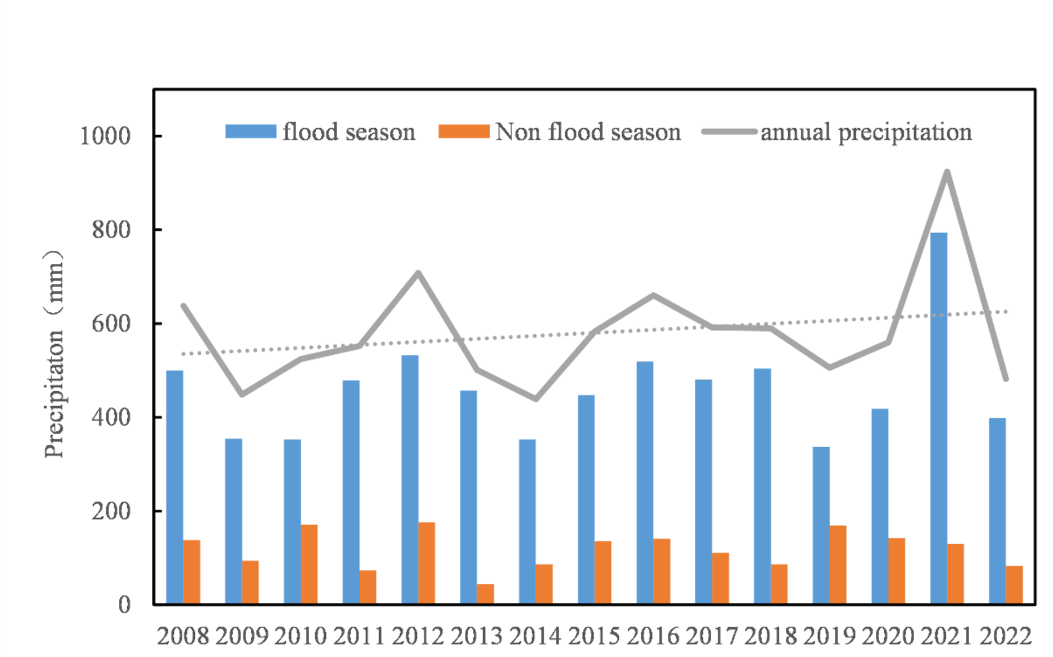

Fig. 3 Precipitation Statistics Table for Beijing Municipality, 2008-2022

Experimental data.

Sentinel-1A data

The research data employed in this study consists of single-look complex (SLC) images from the Sentinel-1A satellite's Interferometric Wide (IW) mode. These images are acquired in ascending orbit, with VV polarization and a spatial resolution of 5m x 20m. The swath width is approximately 250km. The data spans from May 2017 to May 2018, totaling 17 scenes. The precise orbit determination (POD) data used is obtained from GNSS after 21 days of operation (Dai et al., 2016), providing the most accurate orbital information. Each file contains 26 hours of data, covering a full day plus an additional hour before and after. The positioning accuracy of the data is higher than 5cm (Xu et al., 2019).

DEM data

In SAR data processing, DEM data is often required to provide reference terrain or geographic coordinate systems to remove the influence of the terrain phase (Lu et al., 2018). The Shuttle Radar Topography Mission (SRTM) provides a digital elevation model (DEM) of the Earth's surface from NASA. This model includes two types of DEM accuracy: SRTM1 with a 30m resolution and SRTM3 with a 90m resolution. In this study, we selected the SRTM1 with a 30m resolution, which fully covers the study area.

Surface soil moisture data

The surface soil moisture data is extracted from the Global Land Data Assimilation System (GLDAS), available on the EARTHDATA website. For monthly data, the GLDAS Noah Land Surface Model L4 monthly 0.25 x 0.25 degree V2.1 dataset is selected. This dataset includes precipitation, evapotranspiration, soil moisture, temperature, pressure, and other data, providing an approximation of actual soil moisture. The variable SoilMoi0_10cm_inst represents the surface soil moisture content(kg/m^2).

For daily data, the surface soil moisture data is obtained from the GLDAS Catchment Land Surface Model L4 daily 0.25 x 0.25-degree GRACE—DA1 V2.2 dataset, also available on the EARTHDATA website. This dataset includes precipitation rates, surface soil moisture, and other data, which can represent actual soil moisture to some extent. The variable SoilMoi0_S_tavg represents the surface soil moisture content(kg/m^2).

Precipitation Data

The data is sourced from the National Level Ground Meteorological Basic Meteorological Elements Daily Value Dataset of China. This dataset includes daily values of meteorological elements such as pressure, temperature, precipitation, evaporation, relative humidity, wind direction, and wind speed from various meteorological stations across China, including benchmark meteorological stations, basic meteorological stations, and general meteorological stations since January 1951.The dataset comprises data from 12 precipitation monitoring stations. Precipitation data is recorded in units of 0.1mm and is provided in a .txt format. After processing using Python, the data is converted from .txt to .xls format, and monthly average precipitation is calculated

Methodology

SBAS-InSAR principle

The basic principle of SBAS-InSAR technology involves selecting interferometric images with short temporal and spatial baselines for time-series analysis. By choosing such images, SBAS ensures good coherence between images acquired at different times and reduces terrain phase errors, thereby obtaining a stable and reliable sequence of surface deformation. The main methods used in this technology include Singular Value Decomposition (SVD) and least squares estimation to solve equations and obtain surface deformation information for a specific period (Ran et al., 2021).

Assuming there are n+1 SAR images that sufficiently cover the study area, with acquisition times t_0, t_1, ..., t_n, and each image forming interferometric pairs with at least one other image. If N interferograms are formed, then M satisfies the following condition:

$$\frac{n+1}{2} \leq M \leq \frac{n(n+1)}{2}$$

Assuming the initial time is t_0, and the phase difference between any arbitrary time t_i(i=1, ..., n) and t_0 is represented by $\delta_{\varphi(t_j)}$, this parameter is unknown. The differential interferometric phase $\delta_{\varphi(t_j)}$ (j=1,...,n)represents the observation after removing the topographic phase. The interferometric phase of the j interferometric pair is expressed as:

$$\delta_{\varphi_{j(x,\ r)}} = \varphi_{(t_B,\ x,\ r)} - \varphi_{(t_A,\ x,\ r)} \approx \frac{4\pi}{\gamma}[d(t_B,\ x,\ r) - d(t_A,\ x,\ r)$$

Where $d(t_B, x, r)$-$d(t_A, x, r)$ is the Line-Of-Sight (LOS) surface deformation of pixel (x, r) at time t_B relative to time t_A. Γ is the radar wavelength

The radar wavelength can be represented in matrix form as:

$$\delta_\varphi = A_\varphi$$

Where A is the N × n-dimensional coefficient matrix; Φ is the parameter matrix is comprised of the unknown deformation phase values corresponding to the unknown pixels (x, r) at n time points; δ_φ is the matrix formed by the interferometric phase of the unknown pixel (x, r) in M interferometric pairs.

If all interferometric pairs belong to the same small baseline subset, the estimation of cumulative deformation variables can be solved using the least squares method $\hat{\varphi}$:

$$\hat{\varphi} = A^{+}\delta_\varphi, A^{+} = (A^T A)^{-1}A^T$$

The principle of wavelet packet decomposition

Wavelet packet decomposition can simultaneously consider both high-frequency and low-frequency components. It represents wavelet packets using an analysis tree, which utilizes multiple iterations of wavelet transforms to analyze the detailed parts of the input signal. Moreover, it can adaptively select corresponding frequency bands according to the signal characteristics and analysis requirements to match the signal spectrum (Yu et al., 2024).

The decomposition formula is represented as Equation:

$$\begin{cases} d_{j,2n(k)} = \sum h_{i-2k} d_{j+1,n}(i) \\ d_{j,2n(k)} = \sum g_{i-2k} d_{j+1,n}(i) \end{cases}$$

The reconstruction formula is represented as Equation:

$$d_{j+1}(k) = \sum h_{k-2i} d_{j,2n}(i) + \sum g_{k-2i} d_{j,2n+1}(i)$$

Where d is the Decomposition coefficients; h, g is the Filter coefficients; i, k is the Decomposition levels; j, n is the Wavelet packet node numbers.

Data processing

The response of surface soil water content to precipitation

Generally speaking, precipitation directly replenishes the soil moisture content of the surface layer. When there is a sudden change in soil moisture, precipitation is considered as a significant factor (Hu et al., 2019). To explore the relationship between them, the variation in surface soil moisture content and precipitation is shown in Figure 4. From the figure, the surface soil moisture and precipitation generally exhibit a consistent trend, with surface soil moisture increasing as precipitation increases. During periods without precipitation, the surface soil moisture shows a slight downward trend, which may be due to the lack of precipitation replenishment. However, surface soil moisture still contributes to the recharge of other aquifers, leading to a decrease. Additionally, there is a certain lag between the two; the increase in surface soil moisture typically occurs about two days after the precipitation ends.

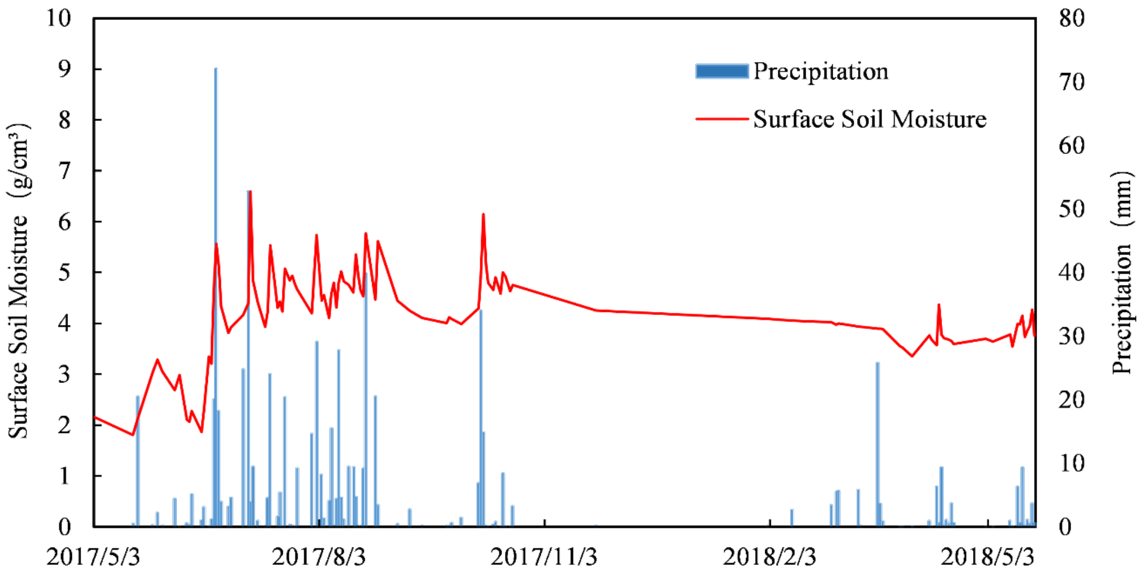

Fig. 4 Surface Soil Moisture and Precipitation Variation Chart

Surface soil water content excluding the influence of precipitation

From the analysis above, it is evident that precipitation has a certain replenishing effect on the surface soil moisture content. Therefore, in order to obtain surface soil moisture data unaffected by precipitation, it is necessary to perform wavelet packet decomposition on the daily surface soil moisture data.

The surface soil moisture content is a time series. The method of signal decomposition is used to optimize time series data to remove the noise impact of precipitation. Signals that are close to the time series of precipitation are selected as precipitation signals to be removed. Therefore, the daily surface soil moisture data is decomposed into different bands to explore the response of different bands to precipitation. The results of the decomposition are shown in Figure 5.

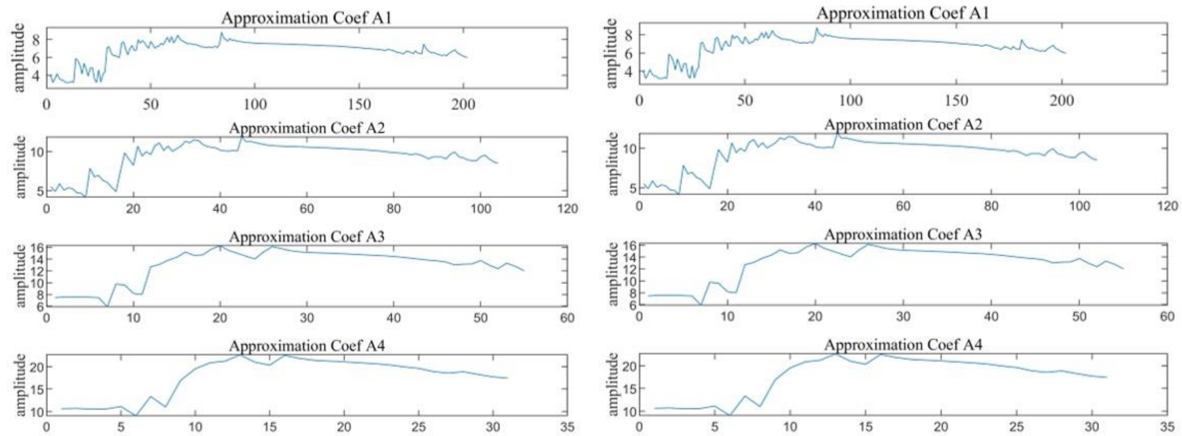

Fig. 5 Decomposed Data of Surface Soil Moisture Content

The decomposed data is reconstructed to obtain the results as shown in Figure 6:

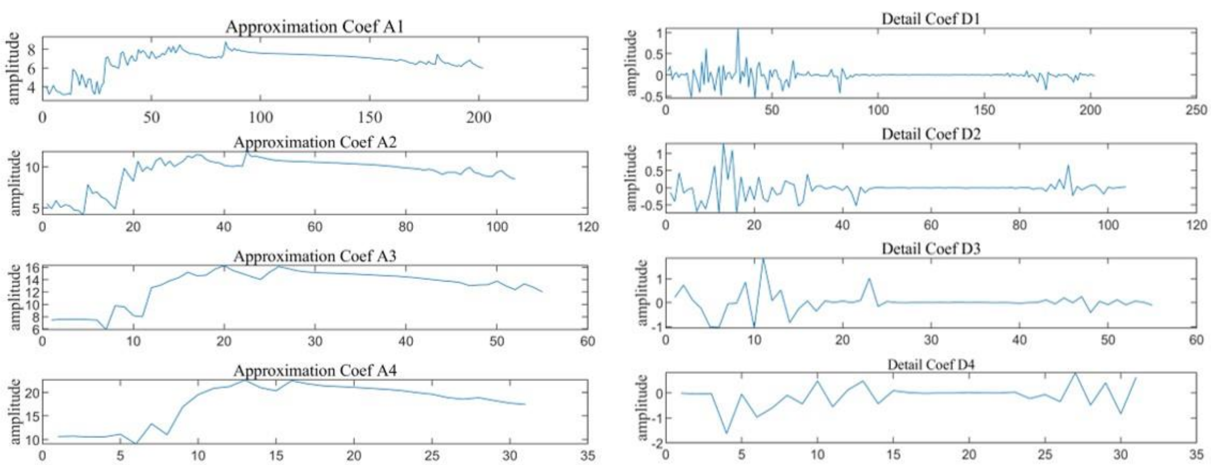

Fig. 6 Reconstructed Data of Surface Soil Moisture Content

The reconstructed data is correlated with precipitation data, and the analysis results are shown in Table 1. Signal D3, which is most similar to the precipitation time series, is removed, leaving behind data with lower response levels. After inverse wavelet transformation, daily surface soil moisture data unaffected by precipitation are obtained, as shown in Figure 7:

Results and Discussion

The causes of land subsidence are quite complex, involving changes in groundwater depth, building loads, lithology, and land use, among other factors. To analyze the factors influencing land subsidence in the study area, this paper conducts a correlation analysis of land subsidence with precipitation and surface soil moisture data.

Table1 Correlation Analysis of Reconstructed Surface Soil Moisture and Rainfall

	Precipitation
D1	0.307**
D2	0.345**
D3	0.393**
D4	0.089
A1	0.321**
A2	0.245**
A3	0.145**
A4	0.129**

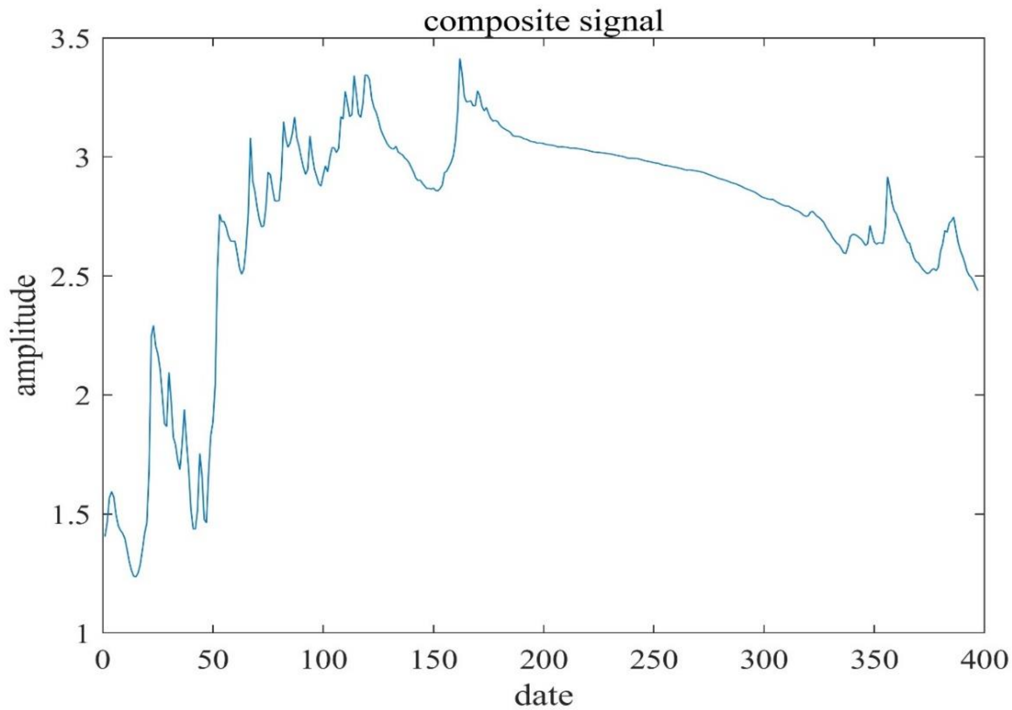

Fig. 7 Merged Data of Surface Soil Moisture Content

Analysis of subsidence results

The program automatically selects the master image for Super-SBAS analysis for May 2017 and May 2018, setting the master image date to December 10, 2017. The spatial baseline threshold is set at 2%, and the temporal baseline threshold is set at 150 days. Through the SBAS-InSAR technique, the annual average deformation velocity map (Figure 7) of the study area is obtained. In the figure, red indicates subsidence, while blue indicates uplift.

From Figure 8, it can be observed that uneven subsidence is prominent in the study area, mainly occurring at the junctions of Haidian-Changping and Chaoyang-Tongzhou. In the Haidian-Changping subsidence area, the main subsidence velocity ranges from -30 to -90 mm/a, with an average of approximately -58 mm/a. The maximum subsidence rate in the subsidence center reaches -81.1 mm/a, with a cumulative maximum subsidence of approximately -88 mm. At the junction of Chaoyang-Tongzhou, there are two subsidence areas: in subsidence area 1, the main subsidence velocity ranges from -120 to -30 mm/a, with an average of approximately -78 mm/a. The maximum subsidence rate in the subsidence center reaches -119.8 mm/a, with a cumulative maximum subsidence of approximately -151 mm. In subsidence area 2, the main subsidence velocity ranges from -145 to -40 mm/a, with an average of -90 mm/a. The maximum subsidence rate reaches -144.3 mm/a, with a cumulative maximum subsidence of approximately -169 mm.

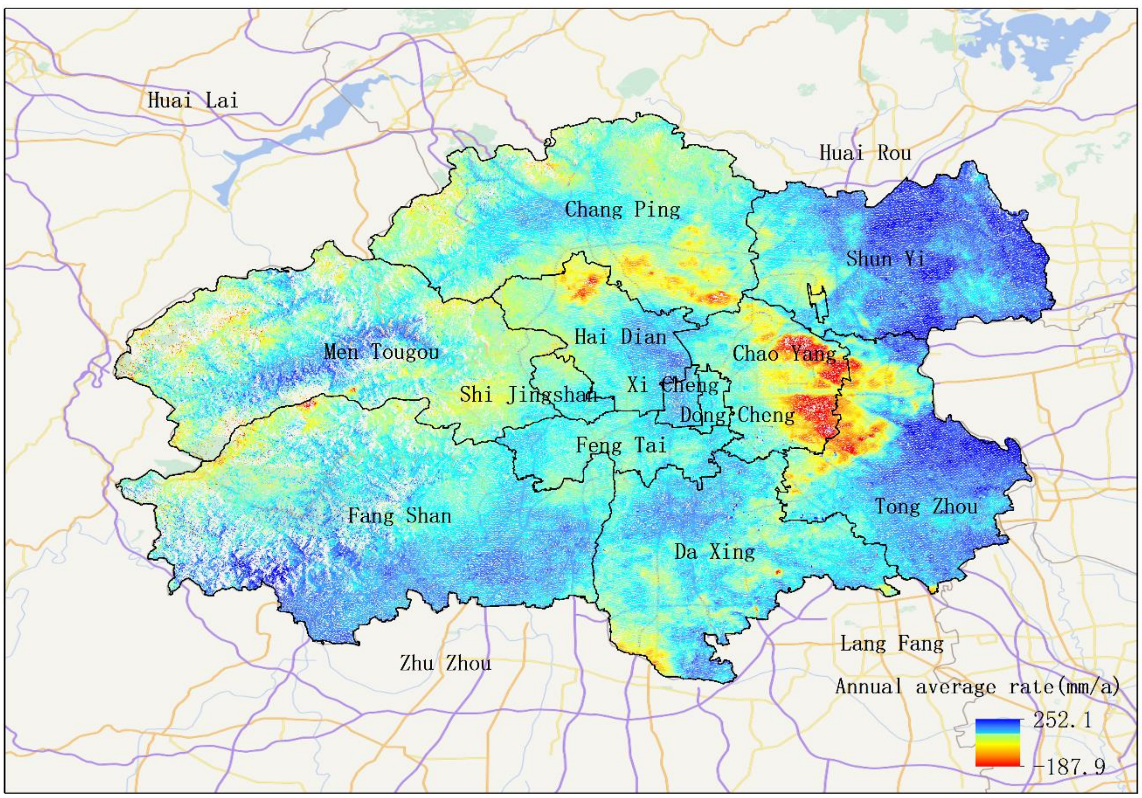

Fig. 8 Annual Average Rate Chart for the Study Area

From the summary and comparison of the various areas, it can be seen that the maximum cumulative subsidence value appears in Mentougou District, which is -238 mm, while the minimum cumulative subsidence value appears in Xicheng District, which is -33 mm.

Table 2 Maximum cumulative settlement and uplift in each district

Area	Maximum cumulative settlement	uplift in each district
Dong Cheng	-40	22
Xi Cheng	-33	24
Feng Tai	-63	152
Shi Jing Shan	-102	48
Hai Dian	-118	60
Tong Zhou	-135	138
Chao Yang	-168	.166
Fang Shan	-192	129
Shun Yi	-62	102
Chang Ping	-153	72
Men Tou Gou	-238	105

The impact of daily surface soil water content on land subsidence

The surface soil moisture content and monthly land subsidence, variations are depicted in Figure 9. From the graph, it can be observed that the surface soil moisture content and land subsidence, exhibit a similar trend to some extent. When the surface soil moisture content decreases, the values of land subsidence, tend to increase.

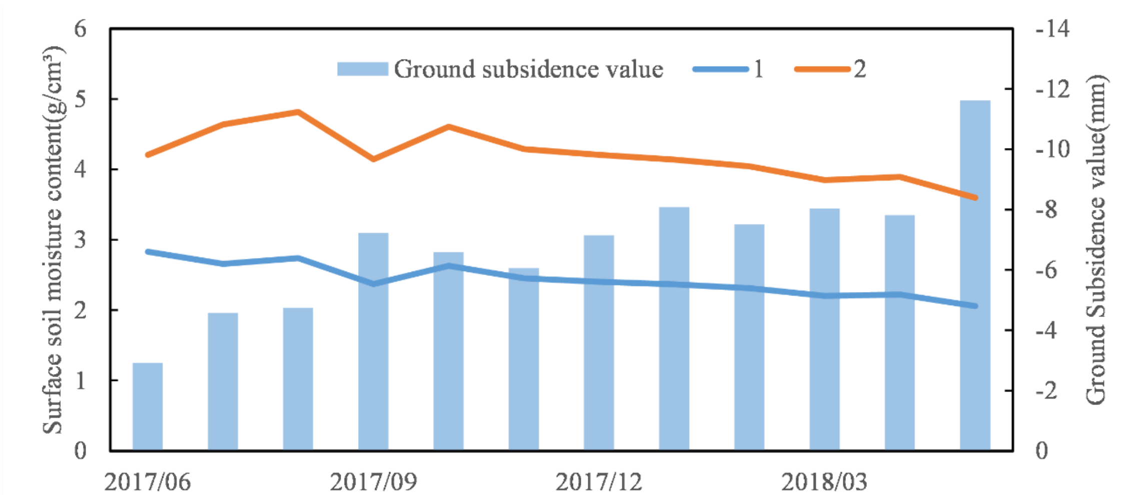

Here's the annotation for the data:
1 is the Surface soil moisture content data after removing the influence of precipitation.
2 is the Surface soil moisture content data without removing the influence of precipitation.

Fig. 9 Surface Soil Moisture and Land subsidence, Variation Chart

The correlation between surface soil moisture content and land subsidence, is illustrated in Figure 10. From the graph, it can be observed that under the influence of precipitation, the correlation between surface soil moisture content and land subsidence, is approximately 0.74, showing a positive correlation. This implies that when surface soil moisture content increases, land subsidence, values decrease, indicating a slowing down of land subsidence. After removing the influence of precipitation, the correlation between surface soil moisture content and land subsidence, values is approximately 0.86, which is stronger than before removing it. This suggests that surface soil moisture content may indeed be a contributing factor to land subsidence.

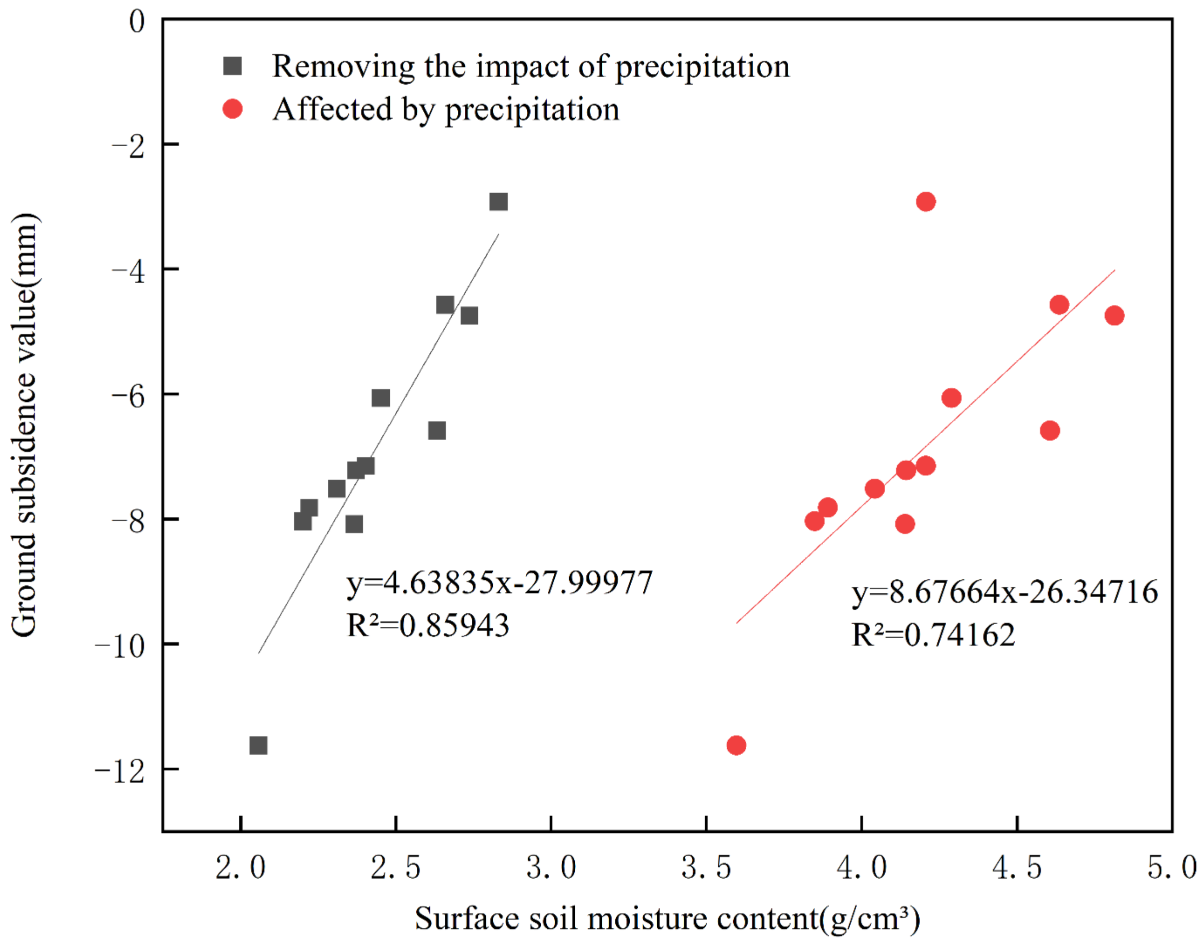

Fig. 10 Relationship Between Surface Soil Moisture and Land subsidence, Chart

The influence of surface soil water content in different seasons on land subsidence

Using monthly surface soil moisture data, the point data is transformed into spatial data using Kriging interpolation. A correlation analysis is then conducted between the spatial data and land subsidence, data. The results are depicted in Figure 11.

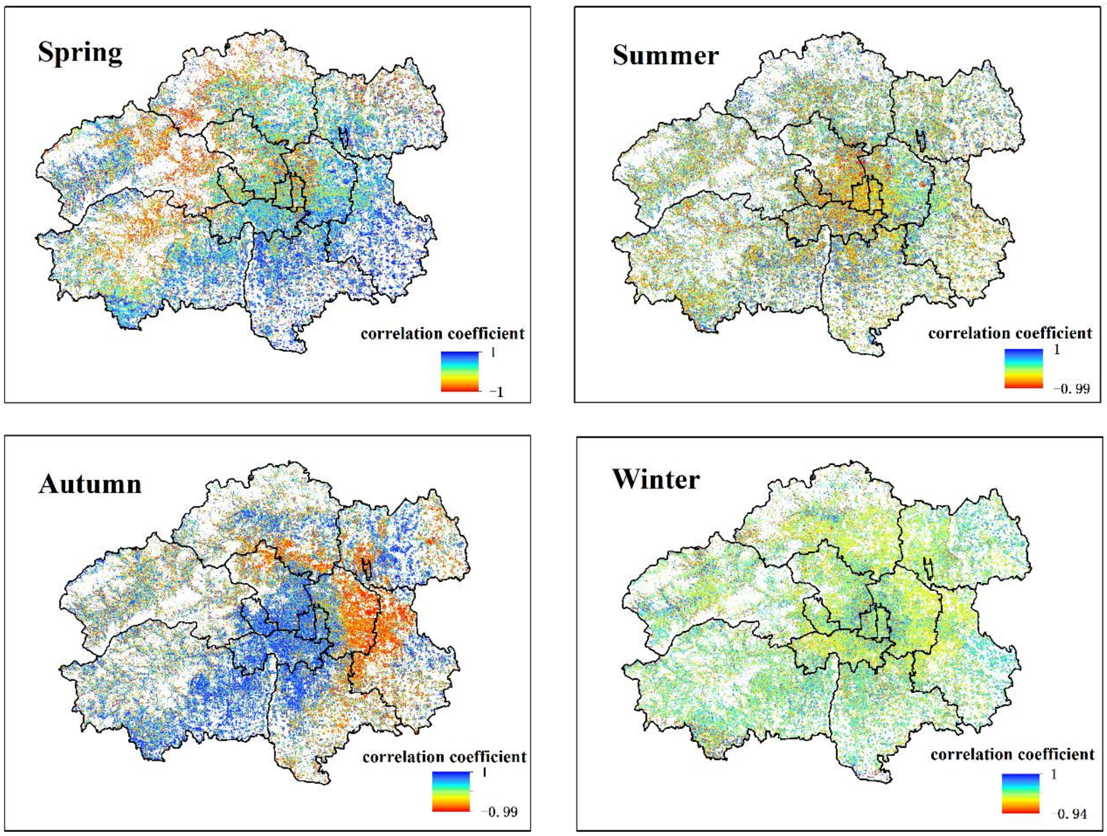

Fig. 11 Correlation between Surface Soil Moisture and Land subsidence, across Different Seasons

(1) Spring: The correlation coefficient between surface soil moisture content and land subsidence, ranges between -1 and 1. In areas where there is a positive correlation, it covers approximately 64.49% of the total study area. Regions exhibiting a high correlation between surface soil moisture content and land subsidence, cover approximately 25.25% of the total study area. Areas with moderate correlation cover about 49.33% of the study area, while those with low correlation cover approximately 25.43%. In most regions, surface soil moisture content and land subsidence, show a positive correlation.

(2) Summer: The correlation coefficient between surface soil moisture content and land subsidence, ranges between -0.99 and 1. In areas where there is a negative correlation, it covers approximately 52.05% of the total study area. Regions exhibiting a high correlation between surface soil moisture content and land subsidence, cover approximately 28.34% of the total study area. Areas with moderate correlation cover about 50.87% of the study area, while those with low correlation cover approximately 20.79%. In most regions, surface soil moisture content and land subsidence, show a negative correlation, indicating that an increase in surface soil moisture content exacerbates land subsidence.

(3) Autumn: The correlation coefficient between surface soil moisture content and land subsidence, ranges between -0.99 and 1. In areas where there is a positive correlation, it covers approximately 58.17% of the total study area. In regions with severe subsidence, surface soil moisture content in autumn shows a significant negative correlation with land subsidence,. However, overall, in most regions of the study area, surface soil moisture content is positively correlated with land subsidence.

(4) Winter: The correlation coefficient between surface soil moisture content and land subsidence, ranges between -0.94 and 1. In areas where there is a positive correlation, it covers approximately 58.17% of the total study area. Areas with low correlation cover about 66.54% of the study area.

The small difference in the correlation between surface soil moisture content and land subsidence, during winter and summer suggests that, under abundant precipitation conditions, the influence of surface soil moisture content on land subsidence, is not very significant. Moreover, in winter, the correlation between surface soil moisture content and land subsidence, exceeding 0.3 covers only 30% of the total study area. Therefore, the influence of surface soil moisture content on land subsidence, during winter is very weak. This preliminary analysis suggests that the limited impact may be due to the lower surface soil moisture content during winter, making its influence on land subsidence, less apparent. Further research could delve into this aspect for deeper analysis.

The impact of precipitation on land subsidence

To explore the relationship between precipitation and land subsidence, daily precipitation data is processed to obtain monthly precipitation data, which is then correlated with monthly land subsidence, data. As shown in Figure 12, there is a positive correlation between precipitation and land subsidence, values, with a correlation coefficient of approximately 0.44. When precipitation increases, land subsidence, values decrease to some extent.

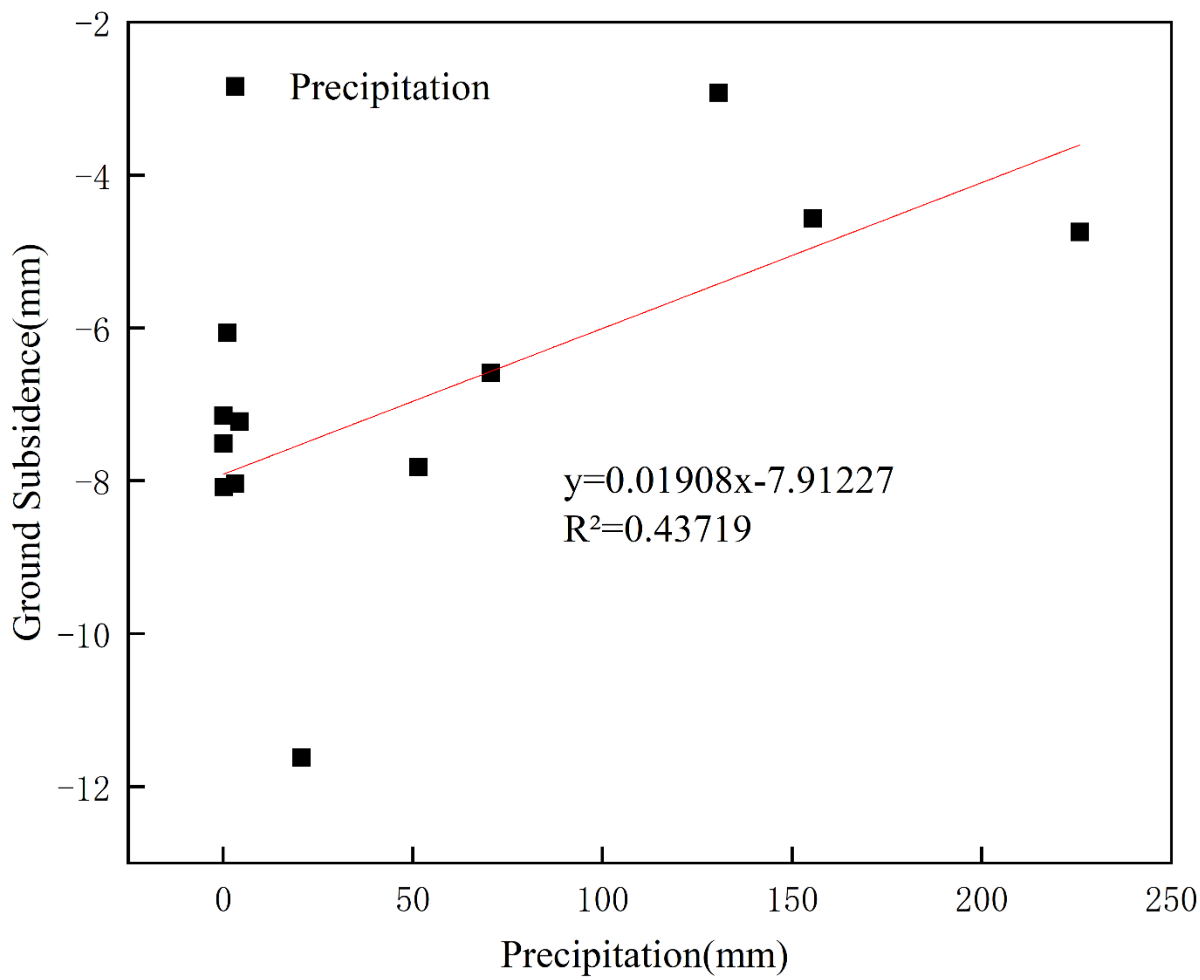

Fig. 12 Relationship Between Precipitation and Land subsidence, Chart

Conclusion

This study utilizes 17 Sentinel-1A images that completely cover the study area and employs the SBAS-InSAR technique to monitor subsidence deformation. It delineates the extent of surface subsidence areas in the study area from May 2017 to May 2018. The main areas of land subsidence within the study area are the Chaoyang-Tongzhou belt and the Haidian-Changping belt. The Chaoyang-Tongzhou belt experiences the most severe subsidence, with a subsidence rate reaching -144.3 mm/a and a maximum cumulative subsidence of -169 mm.The analysis of the maximum cumulative settlement in each district reveals that the maximum cumulative settlement value occurs in Mentougou District, at -238mm, while the minimum cumulative settlement value occurs in Xicheng District, at -33mm. Meanwhile, this paper combines precipitation data and surface soil moisture data to analyze the impact of these factors on ground settlement. Further conclusions are drawn:

(1) Under the influence of precipitation, the surface soil moisture content is positively correlated with land subsidence, with a correlation coefficient of 0.74. After excluding precipitation-affected surface soil moisture data, the correlation between surface soil moisture content and land subsidence, remains positive, with a correlation coefficient of 0.86. This indicates that an increase in surface soil moisture content leads to a decrease in land subsidence values. Therefore, surface soil moisture content alleviates land subsidence to some extent.

(2) The impact of different seasons on land subsidence varies. In most areas, the surface soil moisture content in summer and winter is negatively correlated with land subsidence. However, in most areas, the surface soil moisture content in autumn and spring is positively correlated with land subsidence.

(3) In the study area, there is consistency between precipitation and land subsidence. An increase in precipitation leads to a decrease in land subsidence, thereby alleviating the phenomenon of land subsidence to some extent. It is preliminarily speculated that this is due to the increased replenishment of groundwater caused by increased precipitation, resulting in an elevation of the groundwater table and consequently mitigating ground subsidence.

Reference

Lei, K., Luo, Y., Chen, B., et al, 2016. Distribution Characteristics and Influencing Factors of Land subsidence, in the Beijing Plain Area. J. Geology in China, 43(6), 2216-2228.

Luo, Y., 2017. Preliminary Analysis of Emerging Trends in Land subsidence, in Beijing. J. Shanghai Land & Resources, 38(2), 14-17.

Cheng, L., Wang, X., Zhang, Q., et al, 2018. The impact and trend analysis of the South-to-North Water Diversion Project on land subsidence, in Beijing. J. Yellow River, 40(5), 93-97.

Tian, F., Luo, Y., Zhou, Y., et al, 2017. Temporal and Spatial Contrasts of Land subsidence, and Groundwater Exploitation in Beijing. J. South-to-North Water Transfers ond Water 5cience & Technology, 15(2), 163-169.

Chang, M., Yin, H., Su, G., et al, 2020. Analysis of the Temporal and Spatial Characteristics of Land subsidence, in Tianjin City Using Leveling Data. J. Bulletin of Surveying and Mapping, (7), 88-92.

Lv, L., Liang, W., Liu C., 2021. The application of electronic leveling instruments in subsidence monitoring in mining areas. J. Geomatics & Spatial Information Technology ,44(1), 170-172.

Liu, P., Shen, X., Liu, J., et al, 2020. The application of GPS technology in ground settlement monitoring. J. Geospatial Information, 18(10), 52-54+4-5.

Sun, Y., Liu, S., Gao, R., et al, 2018. Study on Surface Deformation Patterns of Shallow-buried and Wide-vein Shahejinqiu Gold Mine Based on GPS Monitoring. J. Gold, 40(5), 93-97.

Bayik, C., Abdikan, S., Arıkan, M., 2021. Long term displacement observation of the Atatürk Dam,Turkey by multi-temporal InSAR analysis. J. Acta Astronautica, 2021, 189:484-491.

Kim, J., Lin, S., Singh, P., 2021. Underground burning of Jharia coal mine (India) and associated surface deformation using InSAR data. J. International Journal of Applied Earth Observation and Geoinformation, 103, 102524.

Berardino, P., Fornaro, G., Lanari, R., 2002. A new algorithm for surface deformation monitoring based on small baseline differential SAR interferograms. J. IEEE Transactions on Geoscience and Remote Sensing, 40(11), 2375-2383.

Ali, M., 2020. Monitoring the Iran Pol-e-Dokhtar flood extent and detecting its induced ground displacement using sentinel 1 imagery techniques. J. Natural Hazards, 105(3), 1-15.

Wang, S., Zhang, L., Zhou, J., et al. 2023. Research on ground settlement monitoring and its disaster development characteristics in the Honghui mining area of Gansu Province based on SBAS-InSAR time-series analysis technology. J. JOURNAL OF ENGINEERING GEOLOGY, 31(6), 1951-1963.

Song, Y., LI, Y., 2024. Ground deformation monitoring around Dianchi Lake based on SBAS-InSAR. J. Geomatics & Spatial Information Technology, 47(2), 39-42.

Wu, Q., Xie, H., Zhao, Z., 2006. Research on the deformation mechanism of weakly permeable layers. J. Journal of University of Science and Technology Beijing, (3), 207-210.

Yang, J., Li, J., Xiao, G., et al, 2013. The impact of weakly permeable layer drainage on the engineering properties and microstructure of cohesivesoil. J. Geological Science and Technology Information, 32(6), 162-167.

Zhou, X., PU, J., 2002. Experimental study on ground settlement caused by tunnel excavation in sandy soil. J. Rock and Soil Mechanics, (5), 559-563.

Dogan, U., 2005. Land subsidence and caprock dolines caused by subsurface gyPSum dissolutionand the effect of subsidence on the fluvial system in the Upper Tigris Basin (between Bismil-Batman, Turkey). J. Geomorphology, 71(3-4), 389-401.

Sun, J., 2016. Ground Sediment Transport Model and Numerical Simulation. Polish Journal of Environmental Studies. 25(4), 1691-1697.

E, Jian., Sun A., 2007. Mechanism and characteristics of ground settlement in the North China Plain, along with prevention and control measures. J. Resources Environment & Engineering, (2), 156-159.

Dai, X., Shi, C., Lou, Y., 2016. Precise orbit determination and accuracy analysis through multi-GNSS fusion. J Bulletin of Surveying and Mapping, (2), 12-16.

Xu, H., Chen, F., 2019. Tang Panpan, et al. Error correction technique for TOPS mode Sentinel-1 radar interferograms. J. Bulletin of Surveying and Mapping, (10), 114-118.

Lu, Y., Yan, H., Yang, J., et al, 2018. Analysis of the impact of different resolution DEM on the accuracy of InSAR deformation monitoring. J. Journal of Geomatics, 43(6).

Ran, P., Li, S., Yang, X., 2021. Land subsidence, monitoring in Xi'an City based on SBAS-InSAR technology. J. Journal of Henan Polytechnic University (Natural Science), 40(3), 66-74.

Yu, H., Zhu, J., 2024. A denoising algorithm for ultra-wideband radar vital signs signals based on new mode - wavelet packet decomposition. J. Journal of Electronic Measurement and Instrument, 1-10.

Hu, X., Chen, Y., 2019. The dynamics of surface soil moisture variation driven by precipitation. J. Journal of Anhui Agricultural Sciences, 47(21), 58-60.

This paper DOI: 10.5281/zenodo.14025334

Journal New Website web1: https://ijgsw.eu.org/
web2: https://ijgsw.net/
Journal Old Website: http://ijgsw.comze.com/ is no longer used
You can submit your paper to email: Jichao@email.com
Or IJGSW@mail.com